PERGAMON

International Journal of Heat and Mass Transfer 42 (1999) 405–413

International Journal of HEAT and MASS TRANSFER

Experimental evaluation of thermal performance of Gifford–McMahon regenerator using an improved single-blow model with radial conduction

Zei-Chi Chang[a], Min-Sheng Hung[b], Pei-Pei Ding[b], Ping-Hei Chen[b,*]

[a] *Stone Industries Development Center, Hualien, Taiwan*
[b] *Department of Mechanical Engineering, National Taiwan University, No. 1 Roosevelt Rd, Sec. 4, Taipei, Taiwan 10617*

Received 20 October 1997; in final form 30 May 1998

Abstract

An improved single-blow model with nonuniform radial temperature distribution was developed and employed to measure the thermal performance of a Gifford–McMahon regenerator. In the present study, a test facility was established to conduct the single-blow measurement for evaluating the thermal performance of the regenerator with large NTU values (NTU $\geqslant$ 150). A comparison on the NTU value of the test regenerator between this improved model and two prior models is shown. Empirical correlations were presented to show the relationships of the friction factor and the Nusselt number vs. the Reynolds number for the test regenerator.

Nomenclature

A_0 heat conduction area of wire-screen matrix [m^2]
A_{fr} frontal area of wire-screen matrix [m^2]
A_{HT} heat transfer area of wire-screen matrix [m^2]
A_{HT_w} heat transfer area of the tube wall [m^2]
A_w heat conduction area of the tube wall [m^2]
Bi modified Biot number, equation (10)
C_m specific heat of wire-screen matrix [kJ kg^{-1} °C^{-1}]
C_p fluid specific heat at constant pressure [kJ kg^{-1} °C^{-1}]
d_h hydraulic diameter of the wire-screen, equation (20) [m]
d_m wire diameter of the wire-screen [m]
D inner diameter of the tube wall [m]
f friction factor
g shape factor of the porous wire-screen matrix, equation (20)
h average heat transfer coefficient of wire-screen matrix [W m^{-2} K^{-1}]
H_w^* tube wall thickness [m]
J total node number of radial grids
k_f^* conductivity [W m^{-1} K^{-1}]
k_{mr} radial thermal conductivity of wire-screen matrix, equation (9)
k_{mx} axial thermal conductivity of wire-screen matrix, equation (9)
k_s^* conductivity of wire [W m^{-1} K^{-1}]
k_{wr} radial thermal conductivity of tube wall, equation (9)
k_{wx} axial thermal conductivity of tube wall, equation (9)
L regenerator length [m]
$\dot{m}_f$ mass flow rate of fluid [kg s^{-1}]
M_m mass of wire-screen [kg]
NTU number of transfer units of wire-screen matrix or of the heat exchanger, equation (8)
Nu Nusselt number, equation (19)
P dimensionless air pressure
r dimensionless radial distance from the regenerator centerline
r_w aspect ratio, equation (10)
R^* radius of wire-screen [m]
Re_d Reynolds number
R_k conductivity ratio of wire-screen matrix to the tube wall, equation (10)
R_{tc} capacitance of wire-screen matrix to the tube wall, equation (8)

* Corresponding author. Tel.: 00 886 2 362 1522; Fax: 00 886 2 363 1755

0017–9310/98 $19.00
PII: S0017–9310(98)00186–0

R_w dimensionless outer radius of the tube wall
R_w^* outer radius of the tube wall
S_{max} maximum slope of dimensionless exit fluid temperature
t dimensionless time
T dimensionless temperature
T_{fmax} dimensionless heated inlet temperature at the steady state
T_0 dimensionless inlet fluid temperature at $t = 0$
V_0 regenerator total volume [m^2]
x dimensionless axial distance from the inlet of wire-screen matrix.

Greek symbols
ΔP^* pressure drop [N m^{-2}]
ε porosity
μ dynamic viscosity of air [kg m^{-1} s^{-1}]
μ_J Joule–Thomson coefficient
τ dimensionless time constant of inlet fluid temperature at the center.

Superscripts
n node index in time
* dimensional variable.

Subscripts
f fluid
i node index in axial space
j node index in radial space
m wire-screen matrix or the heat exchanger
w tube wall.

Head
$\sim$ predicted value.

1. Introduction

Thermal regenerators have been extensively used in many engineering applications since they were first employed in the cryogenic device at the end of the last century. Because of their many advantageous factors, particularly their superior effectiveness and compactness compared with conventional heat exchangers, they are used in cryocoolers such as the Gifford–McMahon cooler, the Stirling cooler and the pulse-tube cooler.

In prior studies, two types of transient measuring techniques have been commonly employed to measure the average heat transfer rate of a regenerator matrix. One is the single-blow technique [1–4] in which a unidirectional fluid flow is driven through the regenerator matrix. The other is the oscillating (or cyclic) measuring technique [5] in which the flow is driven oscillatingly.

Although, in actual use, the regenerator in most cryocoolers is subjected to an oscillating flow, the measured results obtained by Tanaka et al. [5] showed no significant difference in the regenerator thermal performance from those done under a steady flow. For Reynolds numbers higher than 60, this difference is less than 15%. For simplicity, the present study employed a single-blow technique to evaluate the heat transfer performance of the Gifford–McMahon (G–M) regenerator matrix.

The single-blow technique requires the establishment of a steady flow through the test regenerator matrix. After the steady flow at the upstream of the regenerator matrix is suddenly heated up, histories of both inlet and exit fluid temperatures, assumed to be uniform along the radial direction of the regenerator matrix, are recorded. Once both fluid temperature histories are recorded, an average heat transfer coefficient h is then estimated. The exist temperature history can be predicted by solving the energy equations in the single-blow model for both the matrix and the working fluid, with the given inlet temperature as a boundary condition. This predicted exit temperature history is then compared with the measured one. If these two temperature responses match within specified limits, the assumed h is then considered correct. Two types of matching schemes, the maximum slope and the curve matching schemes, are commonly used for the evaluation of the h value. Detailed discussions of both schemes can be found in Chen and Chang [3]. If the predicted curve does not match the measured one, then another value for h is estimated, and the matching process is iterated until the correct h value is obtained.

However, the whole measured exit flow temperature response could not match well with the predicted one without a precise model to simulate the actual single-blow system. All prior studies have assumed a uniform temperature distribution along the test regenerators in the single-blow model. However, the heat transferred along the direction normal to the fluid flow could be important in the single-blow measurements [7]. The non-uniformity in the fluid temperature over any cross-section through the regenerator also may significantly affect the evaluation of the NTU value of the regenerator matrix in the use of the single-blow measurement.

Thus, the present study aims to propose an improved single-blow model for the use of measuring the thermal performance of the G–M regenerator matrix. The improved model can take account of the radial conduction in both the test regenerator matrix and the fluid flow. Table 1 compares the major characteristics of the single-blow models and the measured NTU range among various single-blow measurements. In addition, a regenerator test facility thereby is also established to conduct the single-blow measurements on the G–M regenerator matrix.

2. Improved single-blow model

Figure 1 shows a schematic view of a single-blow system. In the single-blow measurement, the air flow

Table 1
Characteristics of various single-blow test models

Model	Axial conduction	Radial conduction	Non-adiabatic side wall	J–T Expansion	Inlet fluid temperature	Matching method	Method NTU range
Pucci et al. [8]	Yes	No	No	No	Step	Maximum slope	2.04–25.0
Liang and Yang [6]	No	No	No	No	Exponential rise	Curve matching	0.3–2.2
Mullisen and Lohrke [7]	Yes	No	No	No	Arbitrary	Curve matching	0.45–3.96
Chen and Chang [3]	No	No	Yes	Yes	Arbitrary	Maximum slope	21.0–160.7
Chen and Chang [4]	Yes	No	Yes	Yes	Arbitrary	Maximum slope	120.0–350.0
The present study	Yes	Yes	Yes	Yes	Arbitrary	Maximum slope	151.0–353.8

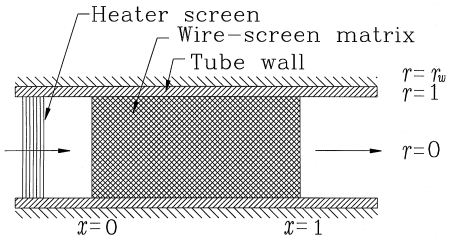

Fig. 1. Schematic view of a single-blow system.

upstream of the test piece, wire-screen matrix, is suddenly heated up. Formulae are derived here to model the heat transfer occurring in the wire-screen matrix. Assumptions made in this model are given as follows:

(1) The air flow is steady and uniform.
(2) The material properties of both matrix and tube wall are constant.
(3) Thermal capacity of the fluid is negligible.
(4) Outer boundary of the tube wall is adiabatic.
(5) The pressure gradient and density of air flow is linear through the matrix.
(6) The Joule–Thomson coefficient is a constant for the air in the matrix.
(7) The fluid free-flow area along the wire-screen matrix is constant.
(8) Heat conduction in the air flow is negligible.

In most prior single-blow models, the tube holding the wire-screen matrix was assumed to be adiabatic and thus there was no need to solve the energy equation for the tube wall [1, 6]. Once the radial conduction along both the tube wall and the wire-screen matrix is taken into account, an additional energy equation for the tube wall appears to assess the heat transfer into the tube wall from both the fluid flow and wire-screen matrix. With the aforementioned assumptions, the dimensionless energy equations are:

$$\frac{\partial T_{\mathrm{f}}}{\partial x}+\mathrm{NTU}(T_{\mathrm{f}}-T_{\mathrm{m}})=\mu_{\mathrm{J}} \tag{1}$$

for the fluid,

$$\frac{\partial T_{\mathrm{m}}}{\partial t}-k_{\mathrm{mx}}\frac{\partial^2 T_{\mathrm{m}}}{\partial x^2}-k_{\mathrm{mr}}\left(\frac{\partial^2 T_{\mathrm{m}}}{\partial r^2}+\frac{1}{r}\frac{\partial T_{\mathrm{m}}}{\partial r}\right)+\mathrm{NTU}(T_{\mathrm{m}}-T_{\mathrm{f}})=0 \tag{2}$$

for the regenerator matrix, and

$$\frac{\partial T_{\mathrm{w}}}{\partial t}-R_{\mathrm{tc}}k_{\mathrm{wx}}\frac{\partial^2 T_{\mathrm{w}}}{\partial x^2}-R_{\mathrm{tc}}k_{\mathrm{wr}}\left(\frac{\partial^2 T_{\mathrm{w}}}{\partial r^2}+\frac{1}{r}\frac{\partial T_{\mathrm{w}}}{\partial r}\right)=0 \tag{3}$$

for the tube wall. The energy equations (1)–(3) are subject to the initial conditions

$$t=0,\quad T_{\mathrm{f}}(x,r,t=0)=T_{\mathrm{m}}(x,r,t=0)=T_{\mathrm{w}}(x,r,t=0)=0-\mu_{\mathrm{J}}\cdot x \tag{4}$$

and boundary conditions for $t>0$

$$x=0,\quad T_{\mathrm{f}}=T_{\mathrm{f_{in}}}(0,r,t),\quad \frac{\partial T_{\mathrm{m}}(0,r,t)}{\partial x}=0,\quad \frac{\partial T_{\mathrm{w}}(0,r,t)}{\partial x}=0$$

$$x=1,\quad \frac{\partial T_{\mathrm{m}}(1,r,t)}{\partial x}=0,\quad \frac{\partial T_{\mathrm{w}}(1,r,t)}{\partial x}=0$$

$$r=0,\quad \frac{\partial T_{\mathrm{m}}(x,0,t)}{\partial r}=0$$

$$r=1,\quad \frac{\partial T_{\mathrm{w}}}{\partial r}=Bi(T_{\mathrm{f}}-T_{\mathrm{w}})+R_k\frac{\partial T_{\mathrm{m}}}{\partial r},\quad T_{\mathrm{m}}(x,1,t)=T_{\mathrm{w}}(x,1,t)$$

$$r=R_{\mathrm{w}},\quad \frac{\partial T_{\mathrm{w}}}{\partial r}=0. \tag{5}$$

The dimensionless variables or parameters in equations (1)–(5) are given as follows:

$$T_{\mathrm{f}}=\frac{T^*_{\mathrm{f}}-T^*_0}{T^*_{\mathrm{fmax}}-T^*_0},\quad T_{\mathrm{m}}=\frac{T^*_{\mathrm{m}}-T^*_0}{T^*_{\mathrm{fmax}}-T^*_0},\quad T_{\mathrm{w}}=\frac{T^*_{\mathrm{w}}-T^*_0}{T^*_{\mathrm{fmax}}-T^*_0} \tag{6}$$

$$t=\frac{t^*}{(M_{\mathrm{m}}C_{\mathrm{m}}/\dot{m}_{\mathrm{f}}C_{\mathrm{P}})},\quad x=\frac{x^*}{L},\quad r=\frac{r^*}{R^*} \tag{7}$$

$$\mathrm{NTU}=\frac{hA_{\mathrm{HT}}}{\dot{m}_{\mathrm{f}}C_{\mathrm{P}}},\quad \mu_{\mathrm{J}}=\frac{\mu_{\mathrm{f}}^*L}{T_{\mathrm{f}\max}^*-T_0^*}\frac{\mathrm{d}P^*}{\mathrm{d}x^*},\quad R_{\mathrm{tc}}=\frac{M_{\mathrm{m}}C_{\mathrm{m}}}{M_{\mathrm{w}}C_{\mathrm{w}}} \tag{8}$$

$$k_{\mathrm{mx}}=\frac{k_{\mathrm{mx}}^*A_0}{\dot{m}_{\mathrm{f}}C_{\mathrm{P}}L},$$

$$k_{\mathrm{mr}}=\frac{k_{\mathrm{mr}}^*\pi L}{\dot{m}_{\mathrm{f}}C_{\mathrm{P}}},\quad k_{\mathrm{wx}}=\frac{k_{\mathrm{w}}^*A_{\mathrm{w}}}{\dot{m}_{\mathrm{f}}C_{\mathrm{P}}L},\quad k_{\mathrm{wr}}=\frac{k_{\mathrm{w}}^*\pi(2R^*-H_{\mathrm{w}}^*)L}{\dot{m}_{\mathrm{f}}C_{\mathrm{P}}H_{\mathrm{w}}^*} \tag{9}$$

$$Bi=\frac{\mathrm{NTU}}{k_{\mathrm{wx}}}\frac{R^*A_{\mathrm{w}}}{LA_{\mathrm{HT}}},\quad r_{\mathrm{w}}=\frac{R^*+H_{\mathrm{w}}^*}{R^*}=\frac{R_{\mathrm{w}}^*}{R^*},\quad R_{\mathrm{k}}=\frac{k_{\mathrm{mr}}^*}{k_{\mathrm{wr}}^*} \tag{10}$$

where R^* and R_{w}^* denotes the radius of the regenerator matrix and the tube wall, H_{w}^* is the tube wall thickness, L is the length of regenerator matrix.

3. Numerical scheme

The present study employs a multistep predictor-corrector finite-difference scheme to solve the governing equations of the single-blow model. This numerical scheme is of second-order accuracy in both time and space.

An explicit finite-difference scheme is used as a predictor to obtain the values of $\tilde{T}_{\mathrm{f}_{i,j}}^{n+1}$, $\tilde{T}_{\mathrm{m}_{i,j}}^{n+1}$ and $\tilde{T}_{\mathrm{w}_{i,j}}^{n+1}$ from the values of $T_{\mathrm{f}_{i,j}}^{n}$, $T_{\mathrm{m}_{i,j}}^{n}$ and $T_{\mathrm{w}_{i,j}}^{n}$ at the previous time step. The superscript in $\tilde{T}_{\mathrm{f}_{i,j}}^{n+1}$, $\tilde{T}_{\mathrm{m}_{i,j}}^{n+1}$ and $\tilde{T}_{\mathrm{w}_{i,j}}^{n+1}$ denotes the $(n+1)$th time step and the subscripts i and j denote the mesh point (i,j) in the two-dimensional computational mesh. Then a Crank–Nicolson scheme as a corrector is iterated several times until the estimated values of $\tilde{T}_{\mathrm{f}_{i,j}}^{n+1}$, $\tilde{T}_{\mathrm{m}_{i,j}}^{n+1}$ and $\tilde{T}_{\mathrm{w}_{i,j}}^{n+1}$ converges with a prescribed error range.

Using the explicit method, the finite-difference forms of equations (2) and (3) are respectively expressed as

$$\begin{aligned}&\frac{\tilde{T}_{\mathrm{m}_{i,j}}^{n+1}-T_{\mathrm{m}_{i,j}}^{n}}{\Delta t}-k_{\mathrm{mx}}\left(\frac{T_{\mathrm{m}_{i+1,j}}^{n}-2T_{\mathrm{m}_{i,j}}^{n}+T_{\mathrm{m}_{i-1,j}}^{n}}{\Delta x^2}\right)\\&-k_{\mathrm{mr}}\left(\frac{T_{\mathrm{m}_{i,j+1}}^{n}-2T_{\mathrm{m}_{i,j}}^{n}+T_{\mathrm{m}_{i,j-1}}^{n}}{\Delta r^2}\right.\\&\left.+\frac{J-1}{j-1}\frac{T_{\mathrm{m}_{i,j+1}}^{n}-T_{\mathrm{m}_{i,j-1}}^{n}}{2\Delta r}\right)+\mathrm{NTU}(T_{\mathrm{m}_{i,j}}^{n}+T_{\mathrm{f}_{i,j}}^{n})=0\end{aligned} \tag{11}$$

$$\begin{aligned}&\frac{\tilde{T}_{\mathrm{w}_{i,j}}^{n+1}-T_{\mathrm{w}_{i,j}}^{n}}{\Delta t}-R_{\mathrm{tc}}k_{\mathrm{wx}}\left(\frac{T_{\mathrm{w}_{i+1,j}}^{n}-2T_{\mathrm{w}_{i,j}}^{n}+T_{\mathrm{w}_{i-1,j}}^{n}}{\Delta x^2}\right)\\&-R_{\mathrm{tc}}k_{\mathrm{wr}}\left(\frac{T_{\mathrm{w}_{i,j+1}}^{n}-2T_{\mathrm{w}_{i,j}}^{n}+T_{\mathrm{w}_{i,j-1}}^{n}}{\Delta r_{\mathrm{w}}^2}\right.\\&\left.+\frac{J-1}{j-1}\frac{T_{\mathrm{w}_{i,j+1}}^{n}-T_{\mathrm{w}_{i,j-1}}^{n}}{2\Delta r_{\mathrm{w}}}\right)=0.\end{aligned} \tag{12}$$

Note that the two equations above are applied for $r>0$. The finite difference equations at singularity $r=0$ may be dealt by using the L'hopital rule.

Using a forward difference to approximate $\frac{\partial T_{\mathrm{f}}}{\partial x}$, equation (1) becomes

$$\begin{aligned}&\frac{T_{\mathrm{f}_{i+1,j}}^{n+1}-T_{\mathrm{f}_{i,j}}^{n+1}}{\Delta x}\\&+NTU\left(\frac{T_{\mathrm{f}_{i+1,j}}^{n+1}+T_{\mathrm{f}_{i,j}}^{n+1}}{2}-\frac{T_{\mathrm{m}_{i+1,j}}^{n+1}+T_{\mathrm{m}_{i,j}}^{n+1}}{2}\right)=\mu_{\mathrm{J}}.\end{aligned} \tag{13}$$

The Crank–Nicolson scheme is applied to equation (2) and (3) as the corrector to yield $T_{\mathrm{m}_{i,j}}^{n+1}$ and $T_{\mathrm{w}_{i,j}}^{n+1}$ as follows:

$$\begin{aligned}T_{\mathrm{m}_{i,j}}^{n+1}=\;&T_{\mathrm{m}_{i,j}}^{n}-\left(\frac{2k_{\mathrm{mx}}\Delta t}{\Delta x^2}+\frac{2k_{\mathrm{mr}}\Delta t}{\Delta r^2}\right.\\&\left.+\mathrm{NTU}\cdot\Delta t\right)\left(\frac{\tilde{T}_{\mathrm{m}_{i,j}}^{n+1}+T_{\mathrm{m}_{i,j}}^{n}}{2}\right)\\&+\frac{k_{\mathrm{mx}}\Delta t}{\Delta x^2}\left(\frac{\tilde{T}_{\mathrm{m}_{i+1,j}}^{n+1}+\tilde{T}_{\mathrm{m}_{i-1,j}}^{n+1}+T_{\mathrm{m}_{i+1,j}}^{n}+T_{\mathrm{m}_{i-1,j}}^{n}}{2}\right)\\&+\frac{k_{\mathrm{mr}}\Delta t}{\Delta r^2}\left(1+\frac{J-1}{j-1}\frac{\Delta r}{2}\right)\\&\times\left(\frac{\tilde{T}_{\mathrm{m}_{i,j+1}}^{n+1}+\tilde{T}_{\mathrm{m}_{i,j-1}}^{n+1}+T_{\mathrm{m}_{i,j+1}}^{n}+T_{\mathrm{m}_{i,j-1}}^{n}}{2}\right)\\&+\mathrm{NTU}\cdot\Delta t\cdot\left(\frac{T_{\mathrm{f}_{i,j}}^{n+1}+T_{\mathrm{f}_{i,j}}^{n}}{2}\right)\end{aligned} \tag{14}$$

$$\begin{aligned}T_{\mathrm{w}_{i,j}}^{n+1}=\;&T_{\mathrm{w}_{i,j}}^{n}-R_{\mathrm{tc}}\left\{\left(\frac{2k_{\mathrm{wx}}\Delta t}{\Delta x^2}+\frac{2k_{\mathrm{wr}}\Delta t}{\Delta r^2}\right)\left(\frac{\tilde{T}_{\mathrm{w}_{i,j}}^{n+1}+T_{\mathrm{w}_{i,j}}^{n}}{2}\right)\right.\\&+\frac{k_{\mathrm{wx}}\Delta t}{\Delta x^2}\left(\frac{\tilde{T}_{\mathrm{w}_{i+1,j}}^{n+1}+\tilde{T}_{\mathrm{w}_{i-1,j}}^{n+1}+T_{\mathrm{w}_{i+1,j}}^{n}+T_{\mathrm{w}_{i-1,j}}^{n}}{2}\right)\\&+\frac{k_{\mathrm{wr}}\Delta t}{\Delta r^2}\left(1+\frac{J-1}{j-1}\frac{\Delta r_{\mathrm{w}}}{2}\right)\\&\left.\times\left(\frac{\tilde{T}_{\mathrm{w}_{i,j+1}}^{n+1}+\tilde{T}_{\mathrm{w}_{i,j-1}}^{n+1}+T_{\mathrm{w}_{i,j+1}}^{n}+T_{\mathrm{w}_{i,j-1}}^{n}}{2}\right)\right\}.\end{aligned} \tag{15}$$

Initial predicted values of $\tilde{T}_{\mathrm{f}_{i,j}}^{n+1}$, $\tilde{T}_{\mathrm{m}_{i,j}}^{n+1}$ and $\tilde{T}_{\mathrm{w}_{i,j}}^{n+1}$ are obtained from the finite-difference equations (11) and (12) in the predictor step and are then substituted into the finite-difference equations (14) and (15) in the corrector step to determine the values of $T_{\mathrm{m}_{i,j}}^{n+1}$ and $T_{\mathrm{w}_{i,j}}^{n+1}$. Using the equation (13) again, the fluid temperature at the $(n+1)$th time step $T_{\mathrm{f}_{i,j}}^{n+1}$ can then be evaluated after the values of $T_{\mathrm{m}_{i,j}}^{n+1}$ and $T_{\mathrm{w}_{i,j}}^{n+1}$ were obtained from equations (14) and (15). At the next iteration, the newly

updated values of $T_{f_{i,j}}^{n+1}$, $T_{m_{i,j}}^{n+1}$ and $T_{w_{i,j}}^{n+1}$ now serve as the predicted values of $\tilde{T}_{f_{i,j}}^{n+1}$, $\tilde{T}_{m_{i,j}}^{n+1}$ and $\tilde{T}_{w_{i,j}}^{n+1}$ in equation (14) and (15) in the corrector step. The iteration can be repeated until the solutions of $T_{f_{i,j}}^{n+1}$, $T_{m_{i,j}}^{n+1}$ and $T_{w_{i,j}}^{n+1}$ converge.

Checking for time and grid independence shows that the calculated temperature response will not vary with the choices at Δt, Δx and Δr if $\Delta t < 0.01$, $\Delta x < 0.03$ and $\Delta r < 0.05$.

4. Data reduction procedure

There are two common matching schemes, the maximum slope and the curve matching schemes, used to match the predicted and measured exit fluid temperature response curves. However, Chen and Chang [3] verified that the uncertainty for the curve matching method is higher than that for the maximum slope scheme for regenerators with high NTU values. Thus, the maximum slope method is used in the present study.

Although there are more parameters in this improved model than there are in the conventional one, the present model still maintains a unique relationship between the NTU and S_{max} of the exit fluid temperature at any given location along the radial direction as long as other parameters are also given. For verifying this, a two-dimensional inlet fluid temperature response is assumed and given by

$$T_f = 1-\exp(-t/\tau), \quad \text{for} \quad r \leqslant 0.6$$
$$T_f = 1-\exp[-t/\tau \times (r/0.6)], \quad \text{for} \quad r > 0.6. \qquad (16)$$

Figure 2 shows the relationship between the maximum slopes of the exit fluid temperature profiles at $r = 0$ and $r = 0.8$ and the NTU value with $R_{tc} = 5$, $r_w = 1.5$, $R_k = 0.1$, $Bi = 0.1$, $\tau = 0.1$, $k_{mx} = 0.001$, $k_{mr} = 0.001$, $k_{wx} = 0.001$ and $k_{wr} = 0.001$. Since the time constant of

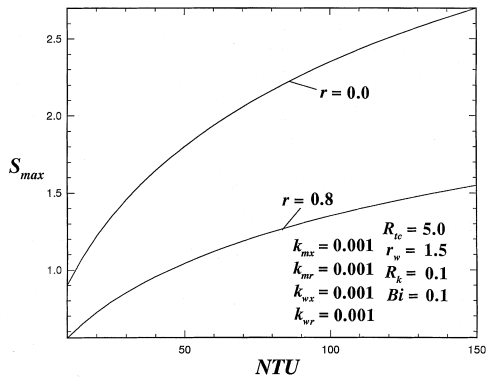

Fig. 2. Relationship between the maximum slopes of the exit field temperature profiles at $r = 0$ and 0.8 and the NTU value with $R_{tc} = 5$, $r_w = 1.5$, $R_k = 0.1$, $Bi = 0.1$, $k_{mx} = 0.001$, $k_{mr} = 0.001$, $k_{wx} = 0.001$ and $k_{wr} = 0.001$.

the inlet temperature at $r = 0$ is smaller than that at $r = 0.8$, the S_{max} of exit fluid temperature at $r = 0$ is always greater than that at $r = 0.8$ for any given NTU. However, the relationship between S_{max} and NTU is still unique.

It is reasonable to expect that the inlet fluid temperature history near the tube wall has a greater time constant to reach the steady state temperature than that at the center. This is due to the heat transfer from the fluid into the tube wall and a coarser heater mesh near the tube wall. In determining the NTU value of the test regenerator matrix, the actual measured inlet fluid temperature histories, however, should be substituted as the inlet condition in the present single-blow model. The above well-behaved inlet fluid temperature histories in equation (16) are only used as a boundary condition to modify present model in obtaining the NTU values by S_{max}, which can also be served as the data bank for future comparison by researchers in related fields.

Note that the exist fluid temperature response may vary with location in the radial direction since the temperature response is distributed two-dimensionally along the regenerator in this model. However, because the temperature response in the central region is usually still uniformly distributed, the location at the center point ($r = 0$) was chosen to represent the exist fluid temperature response in the present study.

5. Experimental apparatus

Based on the improved single-blow test model, a test facility was set up to conduct the transient single-blow measurement. The test facility, as shown in Fig. 3, includes a small air tunnel, a wire-screen heater system, test section and an automated data acquisition system. Air flow was supplied by a compressor. Once a steady flow was established in the air tunnel, the wire-screen heater upstream from the test regenerator was triggered by a personal computer to heat the steady air flow. Meanwhile, time variations of temperature and pressures at the inlet and exit of the test regenerator were measured, digitized and recorded by the automated data acquisition system.

The air tunnel was connected to an air-supply system with a flexible tube. The air-supply system consisted of a reciprocating-type compressor, three PSIΨ company filters, an AD-10 frozen-type air dryer, a regulator and a flexible pipe. The pressure in the chamber of the compressor can be up to 12 atmosphere.

The wire-screen heating system consisted of a pack of 32 wire-screen heaters and four DC power supplies. Each wire-screen heater consisted of a wire screen, two brass electrode bars and one electric insulation layer. The wire screen was made by weaving wires into equally spaced holes in a ring on a printed circuit board. The spacing

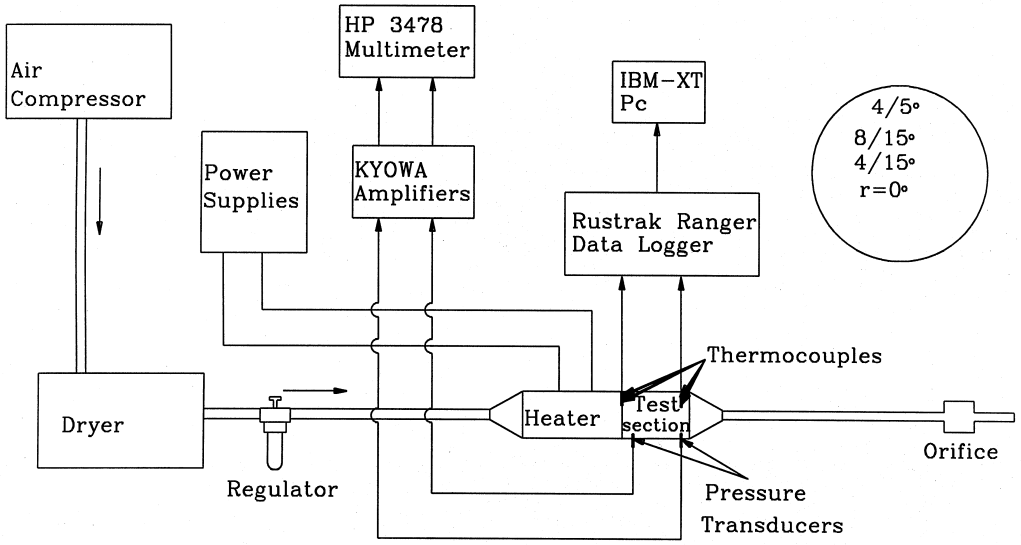

Fig. 3. Single-blow measurement and data reduction system.

between each pair of adjacent wires was only 1.5 mm. The heating wire had a diameter of 0.1 mm and a resistivity of 126.2 $\Omega\ m^{-1}$.

Downstream from the heating system is another flexible tube and a divergent nozzle with an inlet to exit area ratio of 1 : 9 and a third-degree polynomial profile. Two convergent adapters and a pipe adapter were used to fit the cross area change between the wire-screen heater, the test regenerator and the orifice flow meter respectively. In order to conduct the two-dimensional temperature measurement, four thermocouples were installed upstream from the test regenerator and two were installed downstream. The temperature measuring positions were located at a dimensionless radius r of 0.0, 0.27, 0.53, and 0.8 upstream, 0.0 and 0.8 downstream.

The automated data acquisition system was composed of a Rustract Ranger II data logger, two KYOWA CDV-230 amplifiers, an IEEE-488 interface bus, a PC computer and an HP3478 multimeter. The temperature signals were directly recorded by the Rustract Ranger II data logger and were transmitted to and stored in the personal computer by means of the Rustract Ranger II PRONTO software. Two KYOWA PG-20KU pressure transducers were used to measure the inlet and exit pressures of the test regenerator. The voltage was read from the HP3478 multimeter after analog signals were amplified five hundred times through the KYOWA CDV-230 amplifier. Amplifier calibration was conducted by a function generator to assure a linear amplification and zero offset of the signals in the range studied.

The inlet and exit fluid temperature profiles of the test regenerator were measured by YAMALI T-type thermocouples with a diameter of 0.1 mm. The temperature calibration was conducted using a Rustract Ranger II data logger with an uncertainty of $\pm 0.1^{\circ}C$, which affect 0.05% accuracy across the overall span. An EATON UPC5000 pressure calibrator was used to calibrate the two pressure transducers. The uncertainty was under 0.05 psia. A flange-type orifice served as the volumetric flow meter. The calibration for the orifice was conducted in the precision measurement center of ITRI in Taiwan. The uncertainty in volumetric flow measurement was 3%. One G–M regenerator was tested in this work. Physical properties and dimensions of the regenerator are listed in Table 2.

The heat transfer and friction factor measurements

Table 2
Physical properties and dimensions of the test G–M regenerators

Wire-screen material	Bronze
External tube material	Bakelite
Regenerator length [mm]	70
Diameter of wire-screen [mm]	34.2
Tube thickness [mm]	8.7
Mesh number of wire screen	150
C_m [J kg^{-1} K^{-1}]	380
k_s [W m^{-1} K^{-1}	26.0
d_m [mm]	0.10
Number of wire screens	440
M_m [g]	248.9
ε	0.634
d_h [mm]	0.173
M_w [g]	117.3
C_w [J kg^{-1} K^{-1}]	1531

were performed on the G–M regenerator at a range of Re_d from 24 to 150 in the present study. An uncertainty analysis with a 95% confidence interval was carried out according to the method described by Kline and McClintock [9]. The best estimate of uncertainties in Re_d, NTU, h, f and Nu are 4.32, 6.13, 7.50, 5.29 and 8.04% respectively.

6. Results and discussion

Figure 4 shows the measured inlet temperature response curves at different radial locations for the G–M regenerator at $Re_d = 118.87$. The radial temperature distribution is obviously not uniform and varies with time. Since there are thirty grid nodes from $r = 0.0$ to $r = 0.8$ used in the computational mesh for predicting the temperature, the inlet fluid temperatures, at nodes where the fluid temperature responses are not measured, are interpolated from the measured data. Once the inlet fluid temperature response is known, exit fluid temperature curves at different radial locations can be predicted. Based on the measured inlet temperature responses as shown in Fig. 4, Fig. 5 shows both the measured and predicted dimensionless inlet and exit fluid temperature responses for the G–M regenerator. In Fig. 5, the predicted and measured exit fluid temperature responses at both locations of $r = 0.0$ and $r = 0.8$ are shown. The NTU value is determined by matching the maximum slope values of both the predicted and measured exit fluid temperature histories at $r = 0$. As shown in Fig. 5, agreement of the measured and predicted exit temperature curves occurs at both $r = 0.0$ and $r = 0.8$. At $r = 0.8$, the standard deviation between the predicted and measured exit fluid temperatures is less than 9%,

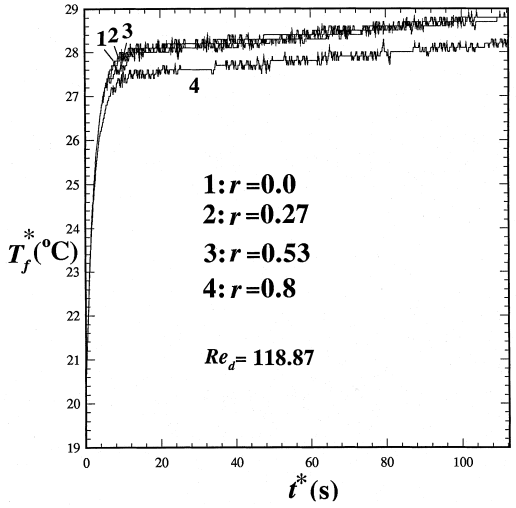

Fig. 4. Measured inlet temperature response curves at different radial locations for the G–M regenerator at $Re_d = 118.87$.

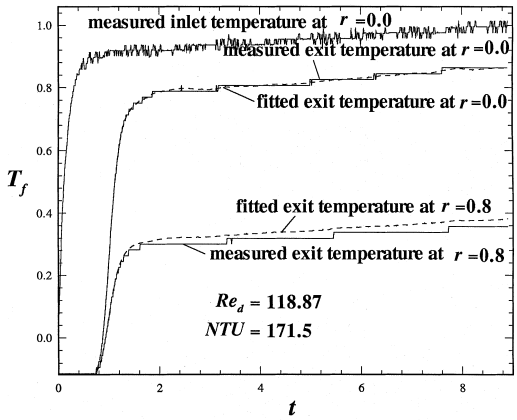

Fig. 5. Measured and predicted dimensionless inlet and exit fluid temperature response for the G–M regenerator at $Re_d = 118.87$.

Measurements were performed on this G–M regenerator and presented in terms of friction factor f and Nusselt number Nu, respectively. Definitions of Re_d, f and Nu are given by

$$Re_d = (\dot{m}_f d_h)/(\mu A_{fr} \varepsilon) \tag{17}$$

$$f = \frac{2\Delta P^* \rho d_h}{(\dot{m}_f/A_{fr}\varepsilon)^2 L} \tag{18}$$

$$Nu = h d_h / k_f. \tag{19}$$

According to the study by Tanaka et al. [5], the hydraulic diameter d_h is defined as

$$d_h = (4\varepsilon d_m)/[g(1-\varepsilon)] \tag{20}$$

where g is the shape factor of the porous wire-screen matrix and is equal to four for the wire screen of the regenerator. The value of effective thermal conductivity of wire-screen matrix is obtained from the empirical equation proposed by Chang [10], which is given by

$$k_m^* = k_f^* (k_s^*/k_f^*)^{(1-\varepsilon)^{0.59}} \tag{21}$$

where k_f^* and k_s^* denotes conductivity of fluid and wire respectively.

Figure 6 shows the friction result for the G–M regenerator compared with those of some prior studies. Observations showed that the G–M regenerator possesses the largest friction factor. As expected, the G–M regenerator also has the best heat transfer performance, which is shown in Fig. 7. For comparison, test results for regenerators packed within 40 wire screens presented by Hamaguchi et al. [1] are also shown. The mesh number of their test regenerator matrices ranges from 10 to 250. However, all NTU values obtained by Hamaguchi [1] are less than 60; much lower than the present values ranging from 150–350. Such a large difference between the NTU values of both studies is due to the number of wire screens

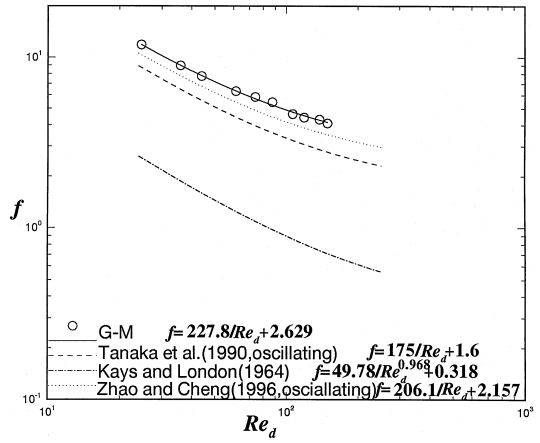

Fig. 6. Friction factor result for the G–M regenerator compared with those of some prior studies.

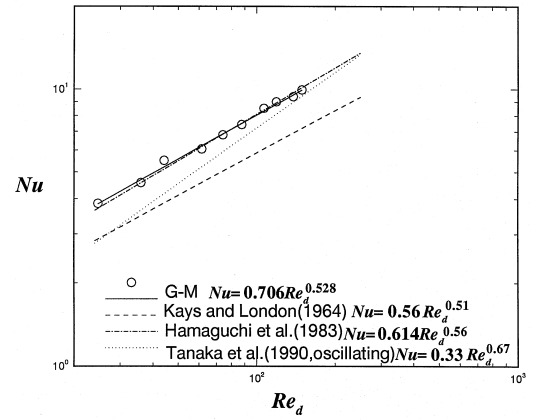

Fig. 7. Heat transfer performance for the G–M regenerator compared with those of some prior studies.

stacked in the wire-screen matrix. Since the heat transfer area increases with the number of wire screens, the measured NTU value of the present test regenerator is much higher than that in their studies. To fit the measured data with the least-square method, the empirical friction factor and heat transfer formulae for the G–M regenerator are

$$f = \frac{227.8}{Re_{\mathrm{d}}} + 2.63 \tag{22}$$

$$Nu = 0.706 Re_{\mathrm{d}}^{0.528}. \tag{23}$$

In order to examine the radial conduction effects in determination of NTU value of the regenerator matrix, two prior single-blow models are also used to obtain the NTU values of the present test G–M regenerator [7]. One is named as 1DA model and neglects the radial conduction of the regenerator matrix and assumes the tube wall is adiabatic. Another one is named as 1DT model[4] which neglects the radial conduction of regenerator matrix too, but has a non-adiabatic tube wall.

All the NTU results obtained by the 1DA, 1DT and present models for the G–M regenerator are listed in Table 3. At the same Reynolds number, the NTU value is highest for the 1DT model but lowest for the 1DA model. Assuming an adiabatic tube wall, the NTU value of the test-wire-screen matrix is underestimated by using the 1DA single-blow model to predict the exit fluid temperature response. On the other hand, the 1DT model overestimates the NTU value of the G–M regenerator matrix. It should be remembered that the temperatures are uniform across the section of the fluid, wire-screen matrix and the tube wall for both 1DA and 1DT models. The discrete temperature jump between the matrix and tube wall may result in a higher heat flux into the tube wall than the actual case. In addition, the error is greater than 8% in determining the NTU value of the present test matrix at NTU > 150 (for 1DT model) if the radial conduction is neglected. More significantly, the error can be greater than 14% if the radial conduction and heat transfers into the tube wall are both neglected (for 1DA model).

7. Conclusions

An improved single-blow model has been developed and employed to measure the thermal performance of one G–M regenerator. In this improved model, nonuniform radial temperature distribution and radial conduction are included. The numerical scheme for this model has also been established. Because the above described effects are included in this model, a more accurate estimated value of NTU of a test regenerator can be obtained, even for a regenerator of rather high NTU value (NTU > 150).

Table 3
Predicted NTU values for the G–M regenerator by 1DA, 1DT and the present models

Re_{d}	NTU (the present model)	NTU (1DA)	NTU (1DT)
24.7	353.9	301.2	373.3
36.0	288.0	246.3	319.8
44.1	282.9	239.4	315.7
61.5	223.0	191.5	245.9
71.2	208.2	178.3	228.5
87.5	192.2	167.9	213.3
106.5	181.2	156.0	201.7
118.9	171.5	147.2	187.6
138.1	154.2	133.8	168.4
149.2	151.0	129.4	164.3

Based on the improved single-blow model, a test facility has also been set up to measure the thermal performance and friction loss of the G–M regenerator. The Reynolds number for the single-blow measurements ranges from 25–150. The maximum-slope method is applied to make the predicted fluid exit temperature curves fit the measured ones. Agreement of the measured and predicted exit temperature curves occurs at both $r = 0.0$ and $r = 0.8$.

Empirical correlations of friction factor and Nusselt number vs. Reynolds number for the wire-screen regenerator are obtained and compared with some test results by prior studies. A comparison between this improved model and two prior models showed that, neglecting the radial conduction and heat transfers into the tube wall would cause an underestimation or overestimation of NTU value of the test regenerator.

References

[1] K. Hamaguchi, S. Takahachi, H. Miyabe, Thermal performance of regenerator matrix, JSME Series B (in Japanese) 49 (1983) 2001–2010.

[2] J. Luna, K.V. Ravilumar, T.H.K. Frederking, Screen heat exchanger performance comparison, Cryogenics 32 (1992) 155–158.

[3] P.H. Chen, Z.C. Chang, Measurements of thermal performance of the regenerator of a cryocooler with high NTU value, Proceedings of the Institution of Mechanical Engineering, Part C Journal of Mechanical Engineering Science 210 (1996) 341–352.

[4] P.H. Chen, Z.C. Chang, Measurements of thermal performance of cryocooler regenerators using an improved single-blow method, International Journal of Heat and Mass Transfer 40 (1997) 2341–2349.

[5] M. Tanaka, I. Yamashita, F. Chisaka, Flow and heat transfer characteristics of Stirling Engine regenerator in oscillating flow, JSME International Journal Series II 33 (1990) 283–289.

[6] C.Y. Liang, W.J. Yang, Modified single-blow technique for performance evaluation on heat transfer surfaces, ASME Journal of Heat Transfer 97 (1975) 16–21.

[7] R.S. Mullisen, R.I. Loehrke, A transient heat exchanger evaluation test for arbitrary fluid inlet temperature variation and longitudinal core conduction, ASME Journal of Heat Transfer 108 (1986) 370–376.

[8] F. Pucci, C.P. Howard, C.H. Piersall, The single-blow transient testing technique for compact heat exchanger surfaces, ASME Journal of Engineering for Power 89 (1967) 29–40.

[9] S.J. Kline, F.A. McClintock, Describing uncertainties in single sample experiments, Mechanical Engineeering 75 (1953) 3–8.

[10] W.S. Chang, Porosity and effective thermal conductivity of wire screens, ASME Journal of Heat Transfer 112 (1990) 5–9.